

# Measurement of signal-to-noise ratios in MR images: Influence of multi-channel coils, parallel imaging, and reconstruction filters

Olaf Dietrich, PhD<sup>1</sup>; José G. Raya, MSc<sup>1</sup>; Scott B. Reeder, MD, PhD<sup>1,2</sup>; Maximilian F. Reiser, MD<sup>1</sup>; Stefan O. Schoenberg, MD<sup>1</sup>

<sup>1</sup>Department of Clinical Radiology – Grosshadern, Ludwig Maximilian University of Munich, Germany

<sup>2</sup>Department of Radiology, University of Wisconsin Madison, WI, USA

## ELECTRONIC PREPRINT VERSION:

*Not for commercial sale or for any systematic external distribution by a third party*

Final version: *J Magn Reson Imaging* 2007; **26**(2): 375–385. <URL:<http://dx.doi.org/10.1002/jmri.20969>>

## ABSTRACT

**PURPOSE:** To evaluate the validity of different approaches to determine the signal-to-noise ratio (SNR) in MRI experiments with multi-element surface coils, parallel imaging, and different reconstruction filters.

**MATERIALS AND METHODS:** Four different approaches of SNR calculation were compared in phantom measurements and in vivo based on (1) the pixel-by-pixel standard deviation in multiple repeated acquisitions, (2) the signal statistics in a difference image, and (3,4) the statistics in two separate regions of a single image employing either the mean value or the standard deviation of background noise. Different receiver coil systems (with 1 and 8 channels), acquisitions with and without parallel imaging, and five different reconstruction filters were compared.

**RESULTS:** Averaged over all phantom measurements, the deviations from the reference value provided by the multiple-acquisitions method are 2.7% (standard deviation 1.6%) for the difference method, 37.7% (25.9%) for the evaluation of the mean value of background noise, and 34.0% (38.1%) for the evaluation of the standard deviation of background noise.

**CONCLUSION:** The conventionally determined SNR based on separate signal and noise regions in a single image will in general not agree with the true SNR measured in images after applying certain reconstruction filters, multi-channel reconstruction, or parallel imaging.

### Keywords:

MR imaging, Image analysis, Signal-to-noise ratio, Parallel imaging, Post-processing filters

### Corresponding author:

Olaf Dietrich, PhD  
Ludwig Maximilian University of Munich  
Department of Clinical Radiology – Grosshadern  
Marchioninistrasse 15, 81377 Munich, GERMANY  
Telephone number: +49 (0)89 7095-3623  
Fax number: +49 (0)89 7095-4627  
E-mail: [od@dtrx.net](mailto:od@dtrx.net)

## INTRODUCTION

The signal-to-noise ratio (SNR) is an important quantity to describe the performance of a magnetic resonance imaging (MRI) system, and is frequently used for image evaluation, measurement of contrast enhancement, pulse sequence and radio frequency coil comparison, and quality assurance. Several methods to determine the SNR of magnetic resonance (MR) images have been described. The most commonly used technique is based on the signal statistics in two separate regions of interest (ROIs) from a single image: one in the tissue of interest to determine the signal intensity, the other in the image background to measure the noise intensity (1,2). There are two important preconditions for SNR measurements based on this “two region” approach: a *spatially* homogeneous distribution of noise over the whole image is required, and the *statistical* intensity distribution of the noise should be known such that the noise measured in a background area can be used to deduce the noise distribution overlaying the anatomic structures in the foreground. These assumptions have been valid for many MR images in past years, in particular if acquired by spin-warp imaging (image reconstruction by 2D or 3D Fourier transform) with a standard single-channel volume quadrature coil followed by a magnitude reconstruction.

However, the use of newly developed phased-array surface coil systems and new reconstruction techniques such as parallel imaging (3,4) can influence both the statistical and the spatial distribution of noise. For instance, the noise distribution in parallel imaging is described by the spatially varying geometry factor (g-factor) and depends on parameters such as coil geometry, phase-encoding direction, and acceleration factor (4,5). In this case, the determination of the noise intensity using a background ROI may lead to inaccurate results and thus to over- or underestimation of SNR. Similarly, the sum-of-squares reconstruction for data from phased-array coils (6) changes the statistical distribution of background noise (7) and even the application of reconstruction filters can influence the spatial distribution of noise. These effects are of particular importance if the SNR is used to compare methods that differently influence the noise distribution such as MRI using non-accelerated vs. parallel-

imaging methods. Nevertheless, in many recently published studies evaluating parallel imaging, e.g. (8–18), SNR calculations were performed using the “two region” approach despite the questionable validity of this method.

The purpose of this study was to evaluate the validity of the “two region” approach in comparison with two alternative techniques in MRI experiments with multi-element surface coils, parallel-imaging techniques and after application of different reconstruction filters, i.e. in situations where an altered probability distribution and an inhomogeneous spatial distribution of background noise must be expected.

## MATERIALS AND METHODS

Phantom experiments were performed on a 1.5-T whole-body MRI system (Magnetom Sonata, Siemens Medical Solutions, Erlangen, Germany) to compare four different methods of SNR measurements in acquisitions with three different pulse sequences, two receiver coil systems, and different reconstruction techniques as described below. To demonstrate the validity of our results *in vivo*, we also performed SNR measurements in a volunteer who provided written informed consent to participate in the study, which had local institutional review board approval.

### Methods of SNR Measurements

Several methods to measure the SNR have been described; they can be differentiated into methods based on a single image, on a pair of images, or on a series of many images. SNR measurements based on two ROIs in a single image (one in the tissue of interest, the other in the image background, i.e., in air, outside the imaged object) can be subdivided into methods using the standard deviation of the background intensity and those using the mean value of the background intensity (1,2). We refer to these “two region” methods as  $\text{SNR}_{\text{stdv}}$  and  $\text{SNR}_{\text{mean}}$ , respectively. With the appropriate conversion factors derived from the noise statistics, both methods yield identical results.

An alternative method of SNR determination is the “difference method” that is based on the evaluation of a difference image of two repeated (identical) acquisitions (19–23); we refer to this approach as  $\text{SNR}_{\text{diff}}$ . A further method based on two images is suggested in the

NEMA standard MS 1-2001 (21) and therefore referred to as  $\text{SNR}_{\text{NEMA}}$ ; it is based on the acquisition of a normal magnitude image and a pure noise image. Recently, Kellman and McVeigh suggested image reconstruction in SNR units (23); this method (referred to as  $\text{SNR}_{\text{units}}$ ) is based on noise measurements in additional noise scans and yields images with pixel intensities directly presenting SNR estimates. Finally, one can employ the most commonly used definition of the SNR of a single image voxel as ratio of the mean value and the standard deviation of the signal intensity time course of the voxel in repeated “identical” acquisitions (5,7,22–25). According to this definition, the noise of a single voxel is described by the stochastic variation of its signal intensity in repeated acquisitions. We refer to this approach as  $\text{SNR}_{\text{mult}}$ . Mathematical descriptions of these methods of SNR determination are presented in the Appendix.

Since  $\text{SNR}_{\text{mult}}$  has the weakest requirements on the statistical and spatial distribution of noise, the validity of other methods can be evaluated by comparing their results to  $\text{SNR}_{\text{mult}}$  as the standard of reference. In this study,  $\text{SNR}_{\text{NEMA}}$  and  $\text{SNR}_{\text{units}}$  were not evaluated because of the technical difficulties involved.  $\text{SNR}_{\text{NEMA}}$  is based on the acquisition and reconstruction of a pure noise image; this cannot be done without modifying the applied pulse sequences as well as the image-reconstruction algorithms and is especially demanding when using auto-calibrating parallel imaging techniques, since noise data must be reconstructed using the same coil sensitivity profiles that were acquired for the image itself. Similarly,  $\text{SNR}_{\text{units}}$  requires pulse sequence modifications to acquire the additional noise scans and a completely new reconstruction algorithm.

### **MRI Acquisition Techniques: RF Coils and Parallel Imaging**

Measurements were performed with a standard single-channel quadrature head coil (1CH) and a dedicated 8-channel surface coil array (8CH) for parallel imaging consisting of 12 coil elements (6 posterior and 6 anterior); 8 of these 12 elements are combined in pairs of 2 such that together with the remaining 4 elements the coil system matches the 8 receiver channels of the MRI system. With the 1CH coil, only non-accelerated acquisitions without parallel imaging were performed. With the 8CH coil, phantom images

were acquired with and without parallel imaging; parallel imaging data was reconstructed using the generalized auto-calibrating partially parallel acquisition (GRAPPA) algorithm (26) and a modified sensitivity-encoding (mSENSE) algorithm (27). For parallel imaging, the acceleration factor was 2 and the number of reference lines used for auto-calibration and the calculation of coil sensitivity profiles was 24.

### **MRI Reconstruction Techniques: Reconstruction Filters**

For all four acquisition techniques, we compared image reconstruction without any additional filtering and with four different reconstruction filters: a Hanning filter, a large-field-of-view (large-FOV) correction filter, an intensity-normalization filter, and an elliptical low-pass filter. The Hanning filter gives higher weighting to central k-space data and lower weighting to peripheral k-space data; this filter can increase the SNR and reduce edge ringing, however, the spatial image resolution is also decreased to a certain degree. The large-FOV compensation filter is used to correct geometric distortions such as “pin-cushion” distortions at the edges of the FOV. The intensity-normalization filter is used to compensate for a spatially varying intensity distribution caused by inhomogeneous coil profiles (typically applied for surface coil systems). The elliptical low-pass filter sets the corners of the k-space to zero, and thus can improve the SNR without substantially decreasing spatial resolution.

### **MRI Pulse Sequences: Imaging Parameters**

Three different pulse sequences were used in this study: a single-shot spin-echo echo-planar-imaging (EPI) sequence, a spin-echo-based single-shot half-Fourier-acquired “rapid acquisition with relaxation enhancement” (hF-RARE) sequence, and a fully gradient-balanced steady-state free-precession (SSFP) sequence. With all 3 sequences, we acquired one slice in transverse orientation with a slice thickness of 8 mm and phase-encoding direction from left to right. The EPI sequence was applied with a matrix of  $192 \times 192$ , TR of 1000 ms, TE of 100 ms, and a bandwidth of 1132 Hz/pixel acquiring 6/8 (75 %) of the k-space in phase-encoding direction (partial-Fourier acquisition). The hF-RARE sequence was applied with a matrix of  $256 \times 256$ , TR of 1000 ms, TE of 75 ms, and a bandwidth of 488 Hz/pixel, acquiring 4/8 (50 %) of the k-

space in phase-encoding direction. The SSFP sequence was applied with a matrix of  $256 \times 256$ , TR of 4.3 ms, TE of 2.15 ms, and a bandwidth of 930 Hz/pixel acquiring the full k-space in phase-encoding direction.

### **Phantom Measurements**

With the three pulse sequences described above, we acquired images of a cylindrical liquid phantom ( $T_1 = 280$  ms,  $T_2 = 240$  ms) with a square FOV of  $300 \times 300$  mm<sup>2</sup> and with 100 repetitions. These measurements were performed with the four acquisition techniques (1CH non-accelerated, 8CH non-accelerated, 8CH GRAPPA, and 8CH mSENSE) and with the five reconstruction techniques (no filter, Hanning filter, large-FOV compensation, intensity normalization, elliptical filter) described above. This resulted in 20 experiments for each of the three evaluated sequences and, thus, in the total number of 60 phantom experiments.

In all of these 60 experiments, we measured the SNR using the four different methods:  $SNR_{mult}$ ,  $SNR_{diff}$ ,  $SNR_{mean}$ , and  $SNR_{stdv}$ .  $SNR_{mult}$  was calculated from repetitions 6 to 100 to avoid any initial non-steady-state images,  $SNR_{diff}$  was calculated from repetitions 6 and 7, and  $SNR_{mean}$  and  $SNR_{stdv}$  were calculated from repetition 6. A linear intensity correction was applied to repetitions 6 to 100 before calculating  $SNR_{mult}$  to compensate for any remaining intensity drift during the acquisition. A square ROI (ROI area  $32 \times 32 = 1024$  pixels) positioned centrally in the phantom was used for SNR calculations with the methods  $SNR_{mult}$  as well as  $SNR_{diff}$ , and to calculate the mean signal intensity for  $SNR_{mean}$  and  $SNR_{stdv}$ . An additional rectangular ROI (ROI area  $64 \times 16 = 1024$  pixels) positioned outside the phantom (close to the image edge in readout direction) was used to calculate the noise intensity for  $SNR_{mean}$  and  $SNR_{stdv}$ . Finally, based on the pixel-by-pixel standard deviation determined for  $SNR_{mult}$ , noise maps displaying this standard deviation as grey-scale image were calculated.

### **In Vivo Measurements**

In vivo measurements were performed in a healthy volunteer (male, 33y) with the SSFP sequence described above. The same acquisition parameters were used except for a larger FOV of  $400 \times 400$  mm<sup>2</sup> and only 10 repetitions to allow breath-hold imaging. The acquired slice was positioned over the upper abdomen

in transverse orientation. We used the conventional body coil for acquisitions with one receiver channel and the 12-element phased-array coil described above for acquisitions with eight receiver channels. By applying the same reconstruction filters as for the phantom measurements, a total number of 20 experiments were performed. In all experiments, we measured the SNR with three different methods:  $SNR_{diff}$  was calculated from repetitions 9 and 10, and  $SNR_{mean}$  as well as  $SNR_{stdv}$  were calculated from repetition 10; the last two repetitions of each acquisition were chosen to avoid any initial non-steady-state effects. A square ROI (ROI area  $20 \times 20 = 400$  pixels) positioned in the liver parenchyma was used for SNR calculations with the method  $SNR_{diff}$ , and to calculate the mean signal intensity for  $SNR_{mean}$  and  $SNR_{stdv}$ . An additional rectangular ROI (ROI area  $40 \times 10 = 400$  pixels) positioned outside the abdomen (close to the image edge in readout direction) was used to calculate the noise intensity for  $SNR_{mean}$  and  $SNR_{stdv}$ .

Since the acquisition of a sufficiently large number of repetitions for  $SNR_{mult}$  is not feasible in breath-hold duration, we did not measure  $SNR_{mult}$  in vivo; instead, we used  $SNR_{diff}$  as the standard of reference and compared the calculated SNR values to  $SNR_{diff}$  to assess the precision of the different methods.

### **Data Evaluation**

All SNR measurements were based on the magnitude image data provided by the standard image reconstruction of the MRI system. We used Bland-Altman plots (28,29) to compare the calculated SNRs to the standard of reference ( $SNR_{mult}$  in the phantom measurements and  $SNR_{diff}$  in the volunteer measurements) and to assess the precision of the different methods. The ratio of the range of the 95 %-confidence interval and the average SNR has been calculated as scalar measure that describes the quality of the method of SNR measurement. In addition, we calculated the relative deviations from the standard of reference, i.e.,  $|SNR_{diff/mean/stdv} - SNR_{mult}| / SNR_{mult}$  for the phantom experiments and  $|SNR_{mean/stdv} - SNR_{diff}| / SNR_{diff}$  for the measurements in vivo. In general, deviations of less than 10 % were considered as acceptable. Finally, we calculated different SNR ratios comparing the 8CH acquisitions without parallel imaging to the 1CH acquisitions, comparing the 8CH acquisition with GRAPPA or mSENSE to the 8CH acquisitions without

parallel imaging, and comparing the acquisitions with each of the four applied reconstruction filters to the acquisitions without filtering. These ratios were calculated for all methods of SNR measurements. For the phantom experiments, we compared these SNR ratios to the results calculated from the standard of reference,  $SNR_{mult}$ , using the Wilcoxon matched-pairs signed-ranks test; in vivo, the number of experiments was too low to allow statistical evaluation.

## RESULTS

### *Phantom Measurements*

Evaluating all 60 phantom measurements, the relative deviations determined for  $SNR_{diff}$  range from 0 % to 7.6 % and, thus, are always lower than 10 %. The relative deviations of  $SNR_{mean}$  range from 0.3 % to 100.4 % and the relative deviations of  $SNR_{stdv}$  from 0 % to 139.9 %. Averaged over all sequences and all measurements, the deviations from  $SNR_{mult}$  are 2.7 % ( $\pm$  standard deviation 1.6 %) for  $SNR_{diff}$ , 37.7 % ( $\pm$  25.9 %) for  $SNR_{mean}$ , and 34.0 % ( $\pm$  38.1 %) for  $SNR_{stdv}$ .

In 53 of all 60 measurements, the deviation of  $SNR_{mean}$  was greater than 10 %. The 7 measurements with deviations lower than 10 % were all performed with the single-channel head coil without parallel imaging. 1 of these 7 measurements was acquired with the hf-RARE pulse sequence (and the intensity normalization filter), the 6 others with the SSFP or EPI pulse sequences and either no filter, the Hanning filter, or the elliptical filter.

In 37 of all 60 measurements, the deviation of  $SNR_{stdv}$  was greater than 10 %; these included all measurements with the large-FOV filter and most of the measurements with the intensity-normalization filter (except in combination with the 8CH coil and

non-accelerated imaging). Of the 23 measurements with deviations lower than 10 %, 21 were performed without parallel imaging and only 2 with mSENSE (and the SSFP pulse sequence combined with the Hanning or intensity normalization filter).

The deviations from  $SNR_{mult}$  are presented as Bland-Altman plots for the three different methods in Fig. 1, showing 95 %-confidence intervals between  $-9.7$  and  $7.0$  for  $SNR_{diff}$ , between  $-116$  and  $114$  for  $SNR_{mean}$ , and between  $-97$  and  $56$  for  $SNR_{stdv}$ . The ratio of the range of the 95 %-confidence interval and the average SNR is 14 % for  $SNR_{diff}$ , 193 % for  $SNR_{mean}$ , and 119 % for  $SNR_{stdv}$ .

The SNR ratios for different acquisition techniques and different reconstruction filters are shown in Table 1; significant differences in comparison to  $SNR_{mult}$  are found for  $SNR_{mean}$  and  $SNR_{stdv}$  and, in one case for  $SNR_{diff}$ . E.g., when applying GRAPPA or mSENSE, the SNR is decreased to about 67 % of its original value without parallel imaging. However, based on  $SNR_{mean}$ , an apparent increase of the SNR to 138 % and 219 % was found. Based on  $SNR_{stdv}$ , the SNR appears increased for GRAPPA and decreased for mSENSE but only to 77 % of its original value. Applying reconstruction filters, significant differences are found for the large-FOV filter:  $SNR_{mult}$  and  $SNR_{diff}$  are unchanged while  $SNR_{mean}$  and  $SNR_{stdv}$  appear increased to 106 % and 116 %, respectively.

Based on the pixel-by-pixel standard deviation determined for  $SNR_{mult}$ , the spatial distribution of noise for different phantom experiments is shown in Fig. 2. The noise is homogeneously distributed in acquisitions without parallel imaging with either no, the Hanning, or the elliptical reconstruction filter. Spatially varying noise levels are found in acquisitions applying either parallel imaging, or the large-FOV or intensity-normalization filter.

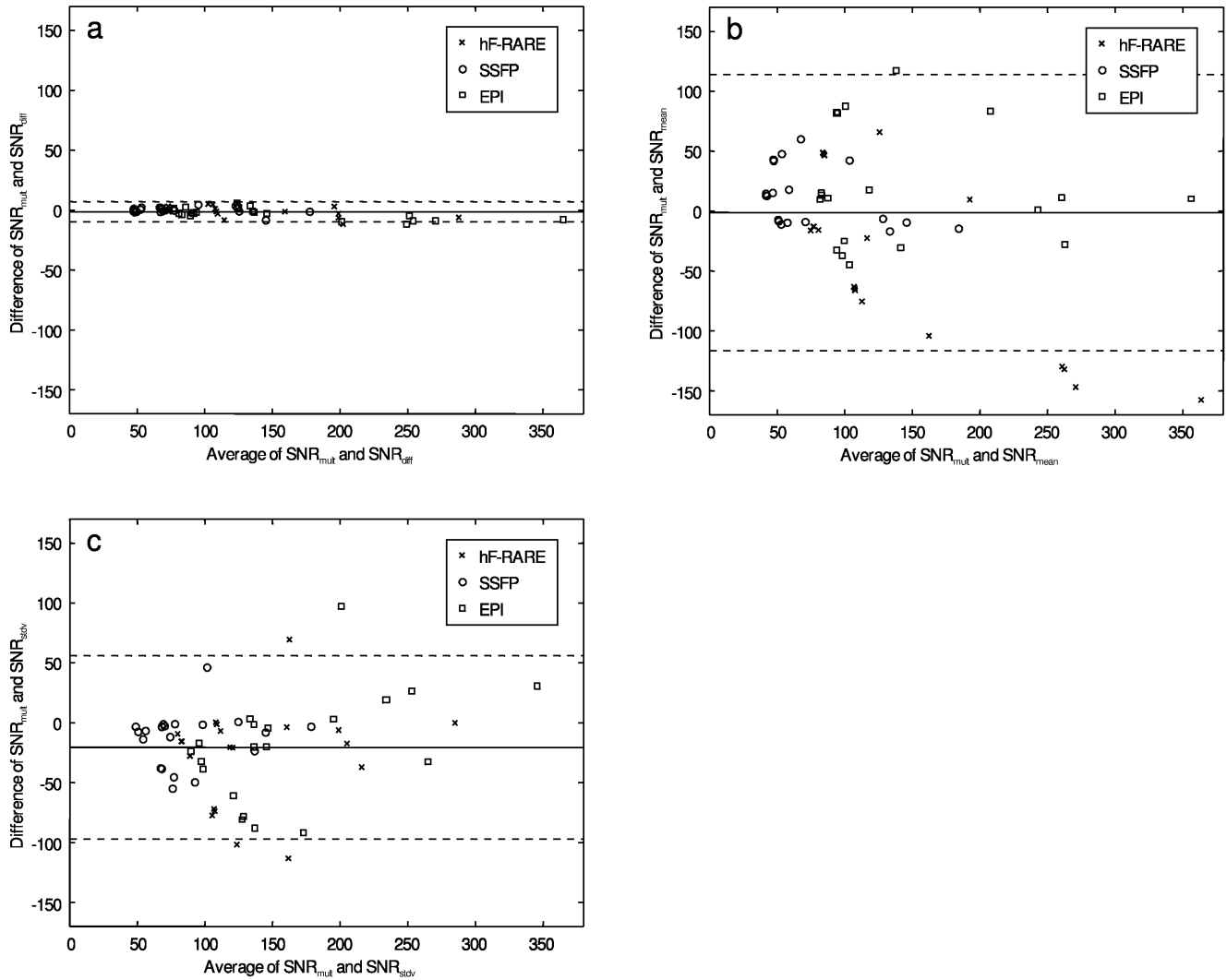


**Figure 1:** Bland-Altman plots showing the agreement between SNR<sub>mult</sub> (the standard of reference) and SNR<sub>diff</sub> (a), SNR<sub>mean</sub> (b), and SNR<sub>stdv</sub> (c) for the phantom measurements. Data for all sequences, acquisition techniques, and reconstruction filters are combined. Note that SNR<sub>diff</sub> agrees much better with SNR<sub>mult</sub> than SNR<sub>mean</sub> and SNR<sub>stdv</sub>.

**Table 1:** SNR ratios (and standard deviations) of different acquisition techniques and reconstruction filters in phantom measurements<sup>a</sup>.

SNR ratio		SNR ratio based on			
		SNR <sub>mult</sub>	SNR <sub>diff</sub>	SNR <sub>mean</sub>	SNR <sub>stdv</sub>
Acquisition technique	SNR(8CH) / SNR(1CH)	54.9% (0.5%)	<b>53.8%</b> (1.6%)	<b>22.4%</b> (5.2%)	<b>62.5%</b> (13.2%)
	SNR(GRAPPA) / SNR(non-accel.)	66.9% (2.9%)	67.1% (4.7%)	<b>138.3%</b> (4.3%)	<b>123.9%</b> (8.6%)
	SNR(mSENSE) / SNR(non-accel.)	66.0% (4.5%)	66.4% (5.7%)	<b>218.5%</b> (15.4%)	<b>76.9%</b> (4.5%)
Reconstruction filter	SNR(Hanning) / SNR(none)	146.4% (7.1%)	145.7% (11.6%)	145.8% (6.3%)	142.0% (6.9%)
	SNR(Large FOV) / SNR(none)	101.1% (2.6%)	101.4% (4.7%)	<b>105.5%</b> (3.4%)	<b>116.1%</b> (4.6%)
	SNR(Normalization) / SNR(none)	100.7% (2.6%)	100.4% (5.4%)	92.3% (18.4%)	91.2% (17.7%)
	SNR(Elliptical) / SNR(none)	107.1% (5.3%)	106.9% (6.6%)	106.4% (6.5%)	107.8% (7.8%)

<sup>a</sup> Significant differences ( $P < 0.05$ ) in comparison to SNR<sub>mult</sub> ratios are emphasized using **bold** figures.

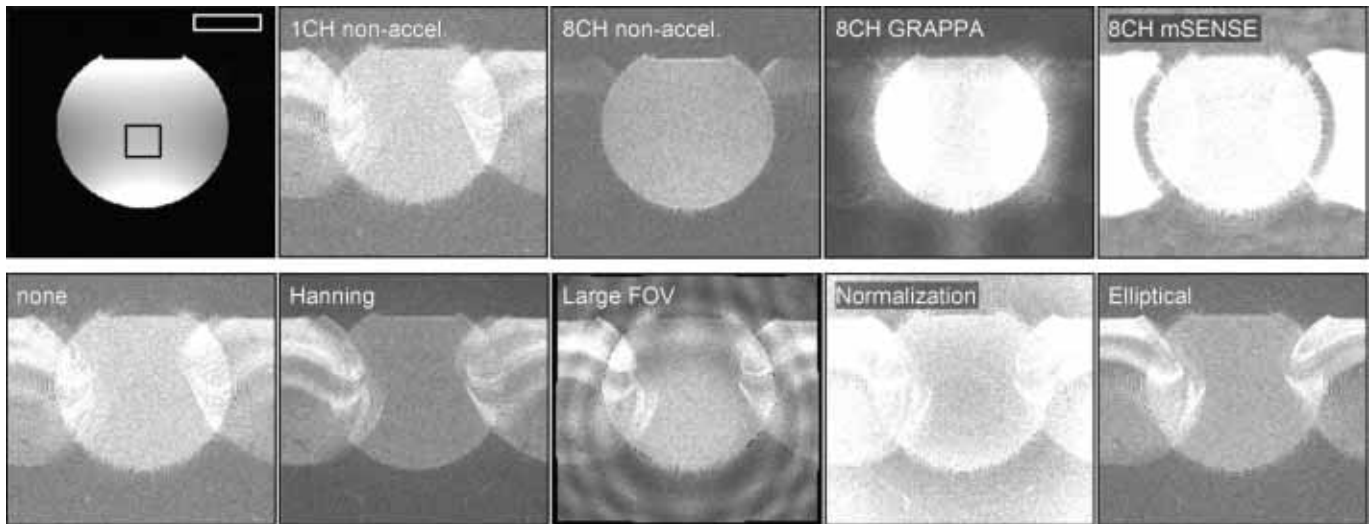


**Figure 2:** ROI positions and spatial noise distribution. The black ROI was used for SNR calculations with the methods  $\text{SNR}_{\text{mult}}$  as well as  $\text{SNR}_{\text{diff}}$ , and to calculate the mean signal intensity for  $\text{SNR}_{\text{mean}}$  and  $\text{SNR}_{\text{stdv}}$ . The white ROI was used to calculate the noise intensity for  $\text{SNR}_{\text{mean}}$  and  $\text{SNR}_{\text{stdv}}$ . The noise maps show the standard deviation calculated pixel-by-pixel from 95 repetitions of an identical acquisition for different acquisition techniques without reconstruction filter (top row) and for different reconstruction filters based on data of the single-channel head coil acquisitions (bottom row).

### ***In Vivo Measurements***

For the measurements *in vivo*, the deviations from the reference measurement,  $\text{SNR}_{\text{diff}}$ , range from 0.8 % to 66.1 % for  $\text{SNR}_{\text{mean}}$  and from 0.1 % to 40.8 % for  $\text{SNR}_{\text{stdv}}$ . Averaged over all measurements, the deviations from  $\text{SNR}_{\text{diff}}$  are 30.1 % ( $\pm$  standard deviation 23.6 %) for  $\text{SNR}_{\text{mean}}$  and 16.0 % ( $\pm$  11.6 %) for  $\text{SNR}_{\text{stdv}}$ .

The deviations of  $\text{SNR}_{\text{mean}}$  were greater than 10 % in 13 of 20 measurements; these include all measurements with the 8CH coil without parallel imaging as well as with GRAPPA. The deviation was lower than 10 % only in the non-accelerated single-channel acquisitions with either no filter, the large-FOV filter, or the elliptical filter and in all filtered mSENSE acquisitions.

The deviations of  $\text{SNR}_{\text{stdv}}$  were greater than 10 % in 13 of 20 measurements as well; these include all GRAPPA measurements, all filtered single-channel measurements, the non-accelerated 8CH measurement without reconstruction filter, and the mSENSE measurements without filter, with the Hanning filter, as well as with the intensity-normalization filter.

The deviations of  $\text{SNR}_{\text{mean}}$  and  $\text{SNR}_{\text{stdv}}$  from  $\text{SNR}_{\text{diff}}$  are presented as Bland-Altman plots in Fig. 3, showing 95 %-confidence intervals between  $-1.8$  and  $5.9$  for  $\text{SNR}_{\text{mean}}$  and between  $-2.3$  and  $2.3$  for  $\text{SNR}_{\text{stdv}}$ . The ratio of the range of the 95 %-confidence interval and the average SNR is 152 % for  $\text{SNR}_{\text{mean}}$ , and 77 % for  $\text{SNR}_{\text{stdv}}$ .

Comparing the SNR ratios for different acquisition techniques and different reconstruction filters in Table 2, similar results as in the phantom experiments are found. E.g., when applying GRAPPA or mSENSE the reference,  $\text{SNR}_{\text{diff}}$ , is decreased to about 75 % and 61 % of its original value without parallel imaging. However, based on  $\text{SNR}_{\text{mean}}$ , an apparent increase of the SNR to 121 % and 150 % is found, and based on  $\text{SNR}_{\text{stdv}}$  the SNR appears unchanged for GRAPPA and decreased for mSENSE to 55 % of its original value.

The subtraction images used to calculate  $\text{SNR}_{\text{diff}}$  are displayed in Fig. 4. They do not show enhanced edge contrast in the area of the liver where the ROI was positioned. Artifacts due to slight misregistrations are visible around the central large vessels, the left lung, and the stomach.

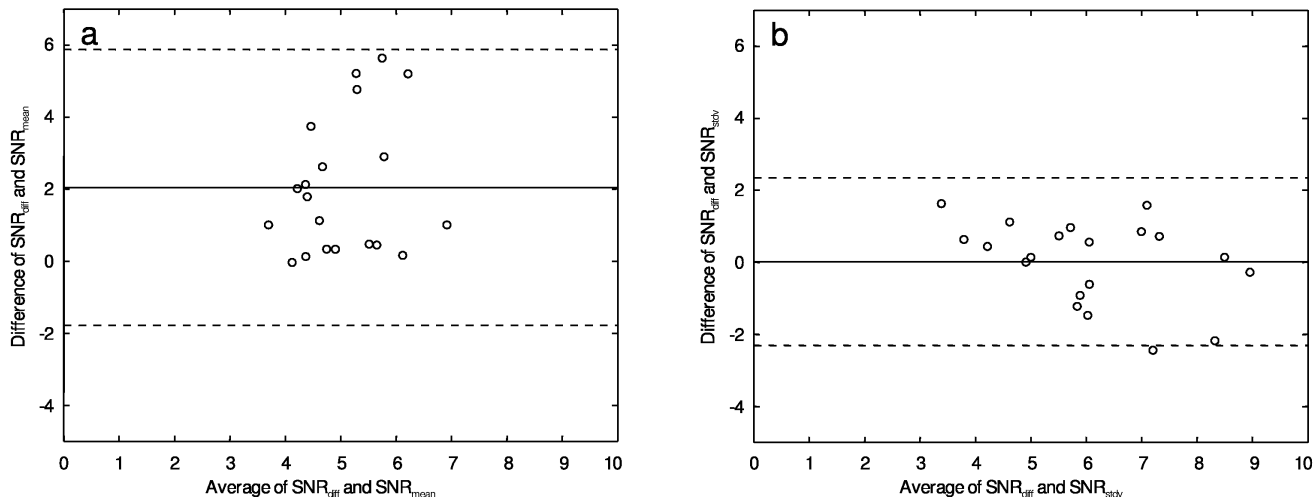


**Figure 3:** Bland-Altman plots showing the agreement between SNR<sub>diff</sub> (the standard of reference) and SNR<sub>mean</sub> (a) as well as SNR<sub>stdv</sub> (b) for the measurements in vivo. Data for all acquisition techniques and reconstruction filters are combined.

**Table 2:** SNR ratios (and standard deviations) of different acquisition techniques and reconstruction filters in measurements in vivo.

SNR ratio		SNR ratio based on		
		SNR <sub>diff</sub>	SNR <sub>mean</sub>	SNR <sub>stdv</sub>
Acquisition technique	SNR(8CH) / SNR(1CH)	135.3% (16.3%)	57.2% (3.9%)	135.3% (5.5%)
	SNR(GRAPPA) / SNR(non-accel.)	74.5% (7.8%)	120.6% (8.7%)	102.8% (9.3%)
	SNR(mSENSE) / SNR(non-accel.)	60.7% (6.8%)	150.1% (18.5%)	54.8% (7.9%)
Reconstruction filter	SNR(Hanning) / SNR(none)	136.0% (16.7%)	148.6% (27.0%)	156.8% (31.7%)
	SNR(Large FOV) / SNR(none)	113.4% (3.5%)	117.2% (17.7%)	146.1% (30.0%)
	SNR(Normalization) / SNR(none)	95.4% (10.2%)	105.3% (18.9%)	103.5% (23.1%)
	SNR(Elliptical) / SNR(none)	105.7% (7.7%)	115.3% (13.9%)	117.2% (26.0%)

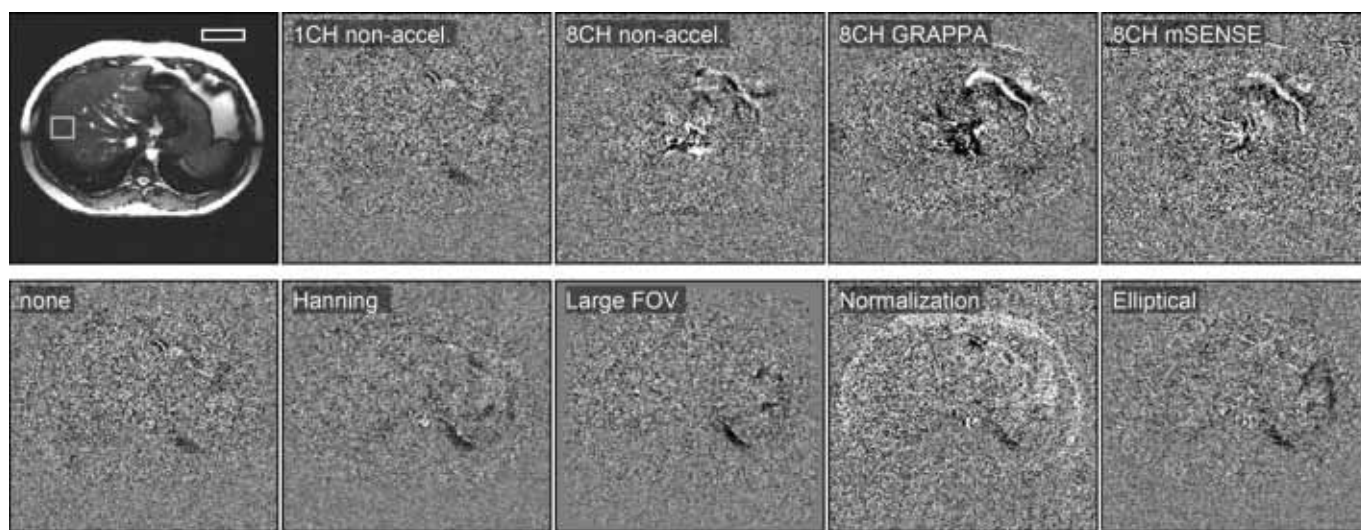


**Figure 4:** ROI positions and difference images. The square ROI was used for SNR calculations with the methods SNR<sub>mult</sub> as well as SNR<sub>diff</sub>, and to calculate the mean signal intensity for SNR<sub>mean</sub> and SNR<sub>stdv</sub>. The rectangular ROI was used to calculate the noise intensity for SNR<sub>mean</sub> and SNR<sub>stdv</sub>. The difference images are calculated from two repetitions of identical acquisitions for different acquisition techniques (top row) and different reconstruction filters (bottom row).



## DISCUSSION

The results presented above demonstrate that, in general, the SNR measured by the “two region” approaches  $SNR_{\text{mean}}$  or  $SNR_{\text{stdv}}$  will not agree with the actual SNR as measured by  $SNR_{\text{mult}}$  and  $SNR_{\text{diff}}$ . This is particularly true after the application of reconstruction filters such as an intensity-normalization filter or large-FOV filter, after multi-channel reconstruction, or after parallel imaging.

For the phantom measurements, the calculated deviations of the three examined methods of SNR measurement from the reference method  $SNR_{\text{mult}}$  show that only the difference method provides accurate results in all measurements with deviations below 10 %. In contrast, both “two region” approaches do not accurately determine the SNR of the acquisitions in most cases with deviations up to 140 %. This is also demonstrated by the Bland-Altman plots with 95 %-confidence intervals that are of comparable width as the actual SNR values for  $SNR_{\text{mean}}$  and  $SNR_{\text{stdv}}$ . To explain these findings both the statistical noise distribution as well as the spatial homogeneity of the noise must be considered.

The statistical noise distribution describes the intensity distribution of the image signal in the presence of noise, i.e., the probability to find a certain deviation from the true signal that would be observed without noise. The original noise in the image raw data prior to its reconstruction with Fourier transformation typically has a normal (or Gaussian) distribution (30). However, this statistical distribution changes during image reconstruction. In the case of reconstructing data from a single receiver channel using the Fourier transform and subsequent magnitude calculation, the background signal of the calculated image is described by the Rayleigh distribution (31). The correction factors used for the determination of  $SNR_{\text{mean}}$  or  $SNR_{\text{stdv}}$  (1,2) are based on the properties of this distribution. Therefore,  $SNR_{\text{mean}}$  or  $SNR_{\text{stdv}}$  can only be expected to be valid methods of SNR calculation if the noise in the image background follows the Rayleigh distribution statistics. In our measurements, this should be the case for single-channel acquisitions with the SSFP and EPI sequence where the deviations of  $SNR_{\text{mean}}$  or  $SNR_{\text{stdv}}$  were less than 10 %. The single-channel acquisitions

of the hF-RARE sequence have a different noise distribution since they were reconstructed as real-part image and negative data was removed by magnitude calculation afterwards; this special reconstruction is based on the Margosian algorithm for half-Fourier data (32).

The 8-channel acquisitions without parallel imaging were reconstructed using the sum-of-squares method (6,33) resulting in a non-central chi-distribution (7) of the signal. This distribution differs considerably from the Rayleigh distribution; in particular the mean value of the background noise is substantially increased. Thus,  $SNR_{\text{stdv}}$  and especially  $SNR_{\text{mean}}$  will fail to determine the true SNR. Similarly, in 8-channel acquisitions with the parallel-imaging algorithms GRAPPA or mSENSE, the noise distribution must be expected to differ from the Rayleigh distribution.

$SNR_{\text{stdv}}$  and in particular  $SNR_{\text{mean}}$  will be considerably biased if the noise intensities are not described by a Rayleigh distribution. Therefore, it is important to verify that the background noise has a Rayleigh distribution before determining  $SNR_{\text{stdv}}$  or  $SNR_{\text{mean}}$ . This can be done by calculating the ratio of the mean value and the standard deviation of the background noise. If this ratio differs significantly from 1.91, the background noise is not described by a Rayleigh distribution and the “two region” approaches should not be used (2).

In addition to a modified statistical noise distribution, the SNR determination in parallel imaging is influenced by the inhomogeneous *spatial* distribution of noise described by the g-factor. Depending on the coil geometry, the noise can be increased or decreased in background regions (Fig. 2) and the SNR may appear lower or higher depending on the positioning of the background ROI when using the “two region” approach. This effect can increase, decrease, or accidentally compensate the SNR bias due to a modified statistical distribution of noise.

Inhomogeneously distributed noise intensities are also causing the deviations of the SNRs with different reconstruction filters. In particular the intensity-normalization filter adds a spatially varying scaling to the image data that influences SNR calculations if different ROIs are used for signal and noise measurements. In the case of the single-channel acquisition this

means that the image intensity in the center is reduced (Fig. 2) resulting in an apparently decreased SNR when using a “two region” approach. The large-FOV filter works by spatially distorting image areas close to the edges of the FOV. Since the noise intensity is measured in those areas,  $\text{SNR}_{\text{mean}}$  and  $\text{SNR}_{\text{stdv}}$  are influenced by this filter as well. In contrast, the Hanning and the elliptical filter do not affect the accuracy of the SNR measurements with the “two region” approach; applying these filters the noise remains homogeneously distributed over the complete image.

It is important to distinguish two different consequences of the observed SNR deviations: The first one is the bias of the determined absolute SNR; however, if this bias can be described by a constant factor for several measurements, the relative change of the SNR may be determined correctly. For example, calculating  $\text{SNR}_{\text{mean}}$  or  $\text{SNR}_{\text{stdv}}$  for a conventional and unfiltered single-channel acquisition as suggested in (1) *without* the appropriate scaling factors given in Eqs. (11) and (12) of the Appendix will result in systematically biased SNR measurements because of the Rayleigh noise distribution. Nevertheless, SNR comparisons for different tissues or pulse sequences remain valid because the constant factor will cancel when calculating any relative SNR change.

However, a second, more problematic consequence must be considered when using the “two region” approach for comparing different acquisition techniques or reconstructions with different filters as in Table 1. In this case, the SNR deviation will in general be different for each acquisition and hence, the SNR change cannot be calculated correctly. This has been illustrated by our 8-channel measurements without parallel imaging, with GRAPPA, and with mSENSE. An SNR decrease due to parallel imaging is to be expected in agreement with the theory providing  $\text{SNR}_R = \text{SNR}_0 / (g\sqrt{R})$  for a geometry factor  $g$  (always  $\geq 1$ ) and an acceleration factor  $R$  (4). For parallel imaging with an acceleration factor of  $R = 2$ , this results in a minimum decrease to  $1/\sqrt{2} \approx 70.7\%$  of the original SNR. While  $\text{SNR}_{\text{mult}}$  and  $\text{SNR}_{\text{diff}}$  demonstrate this expected reduction of the SNR, the *opposite* is found when comparing  $\text{SNR}_{\text{mean}}$  or  $\text{SNR}_{\text{stdv}}$  in non-accelerated acquisitions and with GRAPPA: the SNR appears paradoxically *increased* with parallel imaging! Analogously,  $\text{SNR}_{\text{mean}}$  is apparently increased when

applying mSENSE, while  $\text{SNR}_{\text{stdv}}$  is decreased but to a smaller extent than the reference SNR. This may explain the “somewhat puzzling”  $g$ -factor  $< 1$  reported in (12).

Our measurements in vivo confirm the results of the phantom measurements. As described above, we used  $\text{SNR}_{\text{diff}}$  instead of  $\text{SNR}_{\text{mult}}$  as standard of reference in vivo; apart from practical reasons, this decision was also justified by the results of the phantom measurements, which showed a mean difference of only 2.7 % between both methods.

The measured values of  $\text{SNR}_{\text{diff}}$  show a very similar behavior as in the phantom measurements when comparing 8CH acquisitions without and with parallel imaging, or acquisitions without reconstruction filter and with the Hanning or elliptical filter (Table 2). Applying parallel imaging,  $\text{SNR}_{\text{diff}}$  is substantially decreased, and applying the Hanning or elliptical reconstruction filters, an increased  $\text{SNR}_{\text{diff}}$  is observed. This agreement with the phantom measurements indicates that  $\text{SNR}_{\text{diff}}$  is a valid method to calculate the SNR. In contrast to the phantom measurements, the reference SNR is increased when switching from the conventional single-channel body coil to the 8CH coil. This can be explained by the improved fill factor of the latter.

In general, the measurements in vivo must be expected to be less precise because of the lower reproducibility of each acquisition. Since the calculation of  $\text{SNR}_{\text{diff}}$  is based on a difference image, any remaining respiratory motion or blood flow causes artifacts in the subtraction image, which increases the apparent noise intensity. Nevertheless, the images in Fig. 4 demonstrate that these artifacts remained at low levels in our measurements. The lower reproducibility in subsequent acquisitions, however, is a second reason why  $\text{SNR}_{\text{mult}}$  was not measured in vivo; involuntary patient motion would result in accumulated errors over time and increase the calculated standard deviation, i.e. the apparent noise level.

One of the most important results of the in vivo experiments is the substantial deviation of  $\text{SNR}_{\text{mean}}$  and  $\text{SNR}_{\text{stdv}}$  from the reference SNR especially for the 8CH coil without parallel imaging or with GRAPPA. As in the phantom measurements,  $\text{SNR}_{\text{mean}}$  is paradoxically *increased* when using GRAPPA or mSENSE, and

$SNR_{stdv}$  does not show the true SNR decrease either (Table 2). Therefore, both the phantom measurements and the measurements in vivo indicate that “two region” approaches  $SNR_{mean}$  and  $SNR_{stdv}$  should not be used for SNR determinations in most situations, i.e. in acquisitions using multi-channel phased-array coils, reconstruction filters, or parallel imaging.

In conclusion, our results demonstrate that the signal-to-noise ratio measured by evaluating a foreground and a background region will in general not agree with the true SNR, in particular after the application of certain reconstruction filters, multi-channel reconstruction, or parallel imaging. Consequently, paradoxical results such as an apparent increase of SNR with parallel imaging compared to non-accelerated imaging with identical acquisition parameters may be observed. This result may have important implications for future comparisons of different conventional and parallel-imaging reconstruction methods used for various clinical and methodological studies.

In general, before applying one of the “two region” approaches ( $SNR_{mean}/SNR_{stdv}$ ) it must be verified whether two conditions are (both) fulfilled:

1. The statistical intensity distribution of the background noise must be a Rayleigh distribution. This is the case for magnitude images calculated from a single set of complex raw data.
2. The spatial distribution of noise must be homogeneous. This is the case after conventional standard reconstruction (Fourier transform); however, applying certain reconstruction filters or newer imaging techniques such as parallel imaging or complex iterative image reconstruction methods typically results in an inhomogeneous noise distribution.

Only if these two conditions are fulfilled, the “two region” approaches are valid. It is generally recommended to calculate  $SNR_{stdv}$  rather than  $SNR_{mean}$  because the standard deviation of noise is less variable than its mean value (7).

However, with increasing complexity of MRI systems providing multiple channels and complicated reconstruction algorithms, the number of measurements that fulfill both conditions is decreasing. As soon as reconstruction filters or techniques such as

parallel imaging influence the spatial noise distribution, only those methods of SNR measurements remain valid that determine the noise at the same spatial position as the signal. These are the  $SNR_{diff}$  method, the  $SNR_{NEMA}$  method, the  $SNR_{units}$  method, and the  $SNR_{mult}$  method. Since the  $SNR_{units}$  as well as the  $SNR_{NEMA}$  method require special acquisition and reconstruction techniques, and the  $SNR_{mult}$  method is based on the acquisition of a relatively large number of identical acquisitions, only the  $SNR_{diff}$  method appears feasible for SNR measurements in clinical applications. It should be noted that the  $SNR_{units}$  and  $SNR_{NEMA}$  method (21) are substantially more robust than the calculation of  $SNR_{diff}$ , and it would therefore be highly desirable that the MRI system manufacturers provide support for these methods in future system generations.  $SNR_{mult}$  should be considered as an alternative if pixel-by-pixel measurements (of phantom images) are necessary.

## APPENDIX: DEFINITION OF SNR AND METHODS OF SNR DETERMINATION

An idealized description of the image signal intensity  $S_N$  in the presence of noise in a series of  $K$  repeated acquisitions is given by

$$S_N(\mathbf{r}, k) = S(\mathbf{r}) + N(\mathbf{r}, k), \quad (1)$$

where  $S(\mathbf{r})$  is the “true” image intensity and  $N(\mathbf{r}, k)$  is the superimposed noise in repetition  $k = 1, \dots, K$  and at position  $\mathbf{r} = (x, y, z)$ . For simplicity, we will assume that  $N(\mathbf{r}, k)$  is normally distributed in space (i.e., with respect to  $\mathbf{r}$ ) and in time (i.e., with respect to  $k$ ) and is described by its mean value 0 and its standard deviation  $\sigma$ . (This description of  $S_N(\mathbf{r}, k)$  is valid only for sufficiently large SNRs, i.e.  $S(\mathbf{r}) \gg \sigma$ , otherwise more complicated distributions such as the Rician (2,34–36) or non-central chi-distribution (7) have to be used for  $S_N(\mathbf{r}, k)$ .)

The SNR of a single image voxel at position  $\mathbf{r} = (x, y, z)$  can now be defined as

$$SNR(\mathbf{r}) = \frac{S(\mathbf{r})}{\sigma}. \quad (2)$$

To determine the SNR, two statistical measurements are required: one of the signal intensity  $S$  and one of the original standard deviation  $\sigma$  describing the

noise. While the signal intensity can be calculated as mean value of the signal over all voxels of the ROI and/or all repetitions (the functions  $\text{mean}()$  and  $\text{stddev}()$  return the mean value and the standard deviation of their arguments with respect to the variables and limits below them)

$$S(\mathbf{r}) = \text{mean}_{k=1\dots K}(S_N(\mathbf{r}, k)) = m_K(\mathbf{r}) \quad (3a)$$

$$S(\text{ROI}, k) = \text{mean}_{\mathbf{r} \in \text{ROI}}(S_N(\mathbf{r}, k)) = m_{\text{ROI}}(k) \quad (3b)$$

$$S(\text{ROI}) = \text{mean}_{\substack{k=1\dots K \\ \mathbf{r} \in \text{ROI}}}(S_N(\mathbf{r}, k)) = m_{\text{ROI}, K} \quad (3c)$$

( $m$  as in  $m_K$ ,  $m_{\text{ROI}}$ , or  $m_{\text{ROI}, K}$  is used as abbreviation for a mean value) the determination of  $\sigma$  is more difficult. The most straight-forward method to calculate  $\sigma$  is based on the variation of the signal time course in repeated “identical” acquisitions (5,7,22–25):

$$\begin{aligned} \sigma(\mathbf{r}) &= \text{stddev}_{k=1\dots K}(S_N(\mathbf{r}, k)) \\ &= \text{stddev}(N(\mathbf{r}, k)) = s_K(\mathbf{r}) \end{aligned} \quad (4)$$

( $s$  as in  $s_K$  is used as abbreviation for a standard deviation.) Now, the SNR can be calculated as

$$\begin{aligned} \text{SNR}_{\text{mult}}(\mathbf{r}) &= \frac{S_{\text{mult}}(\mathbf{r})}{\sigma_{\text{mult}}(\mathbf{r})} \\ &= \frac{\text{mean}_{k=1\dots K}(S_N(\mathbf{r}, k))}{\text{stddev}_{k=1\dots K}(S_N(\mathbf{r}, k))} = \frac{m_K(\mathbf{r})}{s_K(\mathbf{r})}, \end{aligned} \quad (5)$$

i.e., as the mean value of the pixel signal with respect to the time series divided by the standard deviation of the pixel signal with respect to the time series (the index “mult” denotes that multiple acquisitions are required to determine the SNR). The SNR of a ROI is given by

$$\begin{aligned} \text{SNR}_{\text{mult}} &= \frac{S_{\text{mult}}}{\sigma_{\text{mult}}} = \frac{\text{mean}_{\mathbf{r} \in \text{ROI}}(m_K(\mathbf{r}))}{\text{mean}_{\mathbf{r} \in \text{ROI}}(s_K(\mathbf{r}))} \\ &= \frac{\text{mean}_{\substack{\mathbf{r} \in \text{ROI} \\ k=1\dots K}}(S_N(\mathbf{r}, k))}{\text{mean}_{\substack{\mathbf{r} \in \text{ROI} \\ k=1\dots K}}(\text{stddev}(S_N(\mathbf{r}, k)))} = \frac{m_{\text{ROI}, K}}{m_{s_K(\mathbf{r})}} \end{aligned} \quad (6)$$

assuming the spatial variation of  $s_K(\mathbf{r})$  can be neglected within the ROI. Described verbally,  $\text{SNR}_{\text{mult}}$  in a ROI is determined as the quotient of the mean value of the signal (this mean value can be calculated with respect to all pixels in the ROI and to all repetitions) and the mean value of the temporal standard deviation of the signal (i.e., first the standard deviation of the signal with respect to the repetitions is calculated for each pixel in the ROI and then averaged within the ROI).

Since repeated acquisitions are time-consuming and may be influenced by systematic signal variations due to patient motion or physiological signal variations, simpler methods requiring fewer acquisitions are typically applied for SNR measurements. Using only two acquisitions  $k_1$  and  $k_2$ , the average SNR in a ROI can be determined as (19–22)

$$\begin{aligned} \text{SNR}_{\text{diff}}(k_1, k_2) &= \frac{S_{\text{diff}}}{\sigma_{\text{diff}}} \\ &= \frac{\frac{1}{2} \text{mean}_{\mathbf{r} \in \text{ROI}}(S_N(\mathbf{r}, k_1) + S_N(\mathbf{r}, k_2))}{\frac{1}{\sqrt{2}} \text{stddev}_{\mathbf{r} \in \text{ROI}}(S_N(\mathbf{r}, k_1) - S_N(\mathbf{r}, k_2))} \\ &= \frac{\frac{1}{2} m_{\text{sum}}}{\frac{1}{\sqrt{2}} s_{\text{diff}}} = \frac{1}{\sqrt{2}} \frac{m_{\text{sum}}}{s_{\text{diff}}}. \end{aligned} \quad (7)$$

Described verbally,  $\text{SNR}_{\text{diff}}$  in a ROI is calculated as the quotient of the mean value (with respect to the ROI) of the signal in the sum image and the standard deviation (evaluated in the same ROI) of the signal in the difference image, divided by the factor  $\sqrt{2}$ . Since Eq. (7) is based on the assumption of a Gaussian noise distribution within the ROI in the difference image, this ROI must be positioned in tissue with sufficiently high SNR (and *not* in the image background).

A second technique suggested in the NEMA standard MS 1-2001 (21) is based on the acquisition of a normal image and a pure noise image. The signal  $S_{\text{NEMA}}$  is calculated as mean value of the normal acquisition  $m_{\text{img}}$ , and the noise  $\sigma_{\text{NEMA}}$  from the standard deviation of the noise image  $s_{\text{noise}}$  multiplied by  $\sqrt{\frac{2}{4-\pi}}$  assuming a Rayleigh distribution and using a ROI at the same position as in the normal image

$$\begin{aligned} \text{SNR}_{\text{NEMA}}(\text{img}, \text{noise}) &= \frac{S_{\text{NEMA}}}{\sigma_{\text{NEMA}}} \\ &= \frac{\text{mean}_{\mathbf{r} \in \text{ROI}_{\text{tissue}}}(S_N(\mathbf{r}, \text{img}))}{\sqrt{\frac{2}{4-\pi}} \text{stddev}_{\mathbf{r} \in \text{ROI}_{\text{tissue}}}(S_N(\mathbf{r}, \text{noise}))} = \frac{m_{\text{img}}}{\sqrt{\frac{2}{4-\pi}} s_{\text{noise}}}. \end{aligned} \quad (8)$$

A disadvantage of this method is that most MRI systems do not permit the acquisition of a pure noise scan with standard pulse sequences. This is especially demanding when using parallel imaging techniques with integrated reference scans like GRAPPA, since the noise data must be reconstructed using the same coil sensitivity profiles that have been acquired for the image itself.

If images are reconstructed in “SNR units” as suggested by Kellman and McVeigh (23), SNR deter-

mination becomes trivial, since the pixel intensities directly represent the SNR and, thus, SNR can be determined for a single pixel or a ROI simply by measuring the pixel intensity

$$\text{SNR}_{\text{units}}(\mathbf{r}) = S_{\text{units}}(\mathbf{r}), \quad (9)$$

or the mean intensity of a ROI

$$\text{SNR}_{\text{units}} = S_{\text{units}} = \text{mean}_{\mathbf{r} \in \text{ROI}}(S_{\text{units}}(\mathbf{r})) = m_{\text{ROI}}. \quad (10)$$

While SNR determination is very simple for images in SNR units, the reconstruction of these images is complicated and requires severe modifications of pulse sequences and reconstruction algorithms as mentioned before.

Finally, most often used for the determination of the SNR are techniques based on the signal statistics in two separate ROIs of a single image  $k$ , one in the tissue of interest ( $\text{ROI}_{\text{tissue}}$ ), the other in the image background ( $\text{ROI}_{\text{air}}$ ) (1,2). The SNR is calculated as

$$\begin{aligned} \text{SNR}_{\text{mean}}(k) &= \frac{S_{\text{mean}}}{\sigma_{\text{mean}}} \\ &= \frac{\text{mean}_{\mathbf{r} \in \text{ROI}_{\text{tissue}}}(S_N(\mathbf{r}, k))}{\sqrt{\frac{2}{\pi}} \text{mean}_{\mathbf{r} \in \text{ROI}_{\text{air}}}(S_N(\mathbf{r}, k))} = \frac{m_{\text{tissue}}}{\sqrt{\frac{2}{\pi}} m_{\text{air}}} \end{aligned} \quad (11)$$

or

$$\begin{aligned} \text{SNR}_{\text{stdv}}(k) &= \frac{S_{\text{mean}}}{\sigma_{\text{stdv}}} \\ &= \frac{\text{mean}_{\mathbf{r} \in \text{ROI}_{\text{tissue}}}(S_N(\mathbf{r}, k))}{\sqrt{\frac{2}{4-\pi}} \text{stddev}_{\mathbf{r} \in \text{ROI}_{\text{air}}}(S_N(\mathbf{r}, k))} = \frac{m_{\text{tissue}}}{\sqrt{\frac{2}{4-\pi}} s_{\text{air}}} \end{aligned} \quad (12)$$

using either the mean value or the standard deviation of the background signal. The correction factors

$$\sqrt{\frac{2}{4-\pi}} \approx 1.53 \quad \text{and} \quad \sqrt{\frac{2}{\pi}} \approx 0.80 \quad \text{in Eqs. (11) and (12)}$$

are required because of the Rayleigh distribution of background noise in magnitude images (31).

## REFERENCES

1. Kaufman L, Kramer DM, Crooks LE, Ortendahl DA. Measuring signal-to-noise ratios in MR imaging. *Radiology* 1989;173:265–267.
2. Henkelman RM. Measurement of signal intensities in the presence of noise in MR images. *Med Phys* 1985;12:232–233.
3. Sodickson DK, Manning WJ. Simultaneous acquisition of spatial harmonics (SMASH): fast imaging with radiofrequency coil arrays. *Magn Reson Med* 1997;38:591–603.
4. Pruessmann KP, Weiger M, Scheidegger MB, Boesiger P. SENSE: sensitivity encoding for fast MRI. *Magn Reson Med* 1999;42:952–962.
5. Sodickson DK, Griswold MA, Jakob PM, Edelman RR, Manning WJ. Signal-to-noise ratio and signal-to-noise efficiency in SMASH imaging. *Magn Reson Med* 1999;41:1009–1022.
6. Roemer PB, Edelstein WA, Hayes CE, Souza SP, Mueller OM. The NMR phased array. *Magn Reson Med* 1990;16:192–225.
7. Constantinides CD, Atalar E, McVeigh ER. Signal-to-noise measurements in magnitude images from NMR phased arrays. *Magn Reson Med* 1997;38:852–857. (Erratum in: *Magn Reson Med* 2004;52:219.)
8. Hagspiel KD, Yao L, Shih MC, Burkholder B, Bissonette E, Harthun NL. Comparison of multistation MR angiography with integrated parallel acquisition technique versus conventional technique with a dedicated phased-array coil system in peripheral vascular disease. *J Vasc Interv Radiol* 2006;17:263–269.
9. Vogt FM, Antoch G, Hunold P, Maderwald S, Ladd ME, Debatin JF, Ruehm SG. Parallel acquisition techniques for accelerated volumetric interpolated breath-hold examination magnetic resonance imaging of the upper abdomen: assessment of image quality and lesion conspicuity. *J Magn Reson Imaging* 2005;21:376–382.
10. Kuhl CK, Gieseke J, von Falkenhausen M, Textor J, Gernert S, Sonntag C, Schild HH. Sensitivity encoding for diffusion-weighted MR imaging at 3.0 T: intraindividual comparative study. *Radiology* 2005;234:517–526.
11. de Vries M, Nijenhuis RJ, Hoogeveen RM, de Haan MW, van Engelshoven JM, Leiner T. Contrast-enhanced peripheral MR angiography using SENSE in multiple stations: feasibility study. *J Magn Reson Imaging* 2005;21:37–45.
12. Chen Q, Quijano CV, Mai VM, Krishnamoorthy SK, Li W, Storey P, Edelman RR. On improving temporal and spatial resolution of 3D contrast-enhanced body MR angiography with parallel imaging. *Radiology* 2004;231:893–899.
13. Fink C, Puderbach M, Bock M, Lodemann KP, Zuna I, Schmahl A, Delorme S, Kauzcor HU. Regional lung perfusion: assessment with partially parallel three-dimensional MR imaging. *Radiology* 2004;231:175–184.
14. Ruel L, Brugieres P, Luciani A, Breil S, Mathieu D, Rahmouni A. Comparison of in vitro and in vivo MRI of the spine using parallel imaging. *AJR Am J Roentgenol* 2004;182:749–755.
15. Hunold P, Maderwald S, Ladd ME, Jellus V, Barkhausen J. Parallel acquisition techniques in cardiac cine magnetic resonance imaging using TrueFISP sequences: comparison of image quality and artifacts. *J Magn Reson Imaging* 2004;20:506–511.
16. Yoshioka H, Sato J, Takahashi N, Lou D, Yamaguchi M, Saida Y, Itai Y. Dual double arterial phase dynamic MR imaging with sensitivity encoding (SENSE): which is better for diagnosing hypervascular hepatocellular carcinomas, in-phase or opposed-phase imaging? *Magn Reson Imaging* 2004;22:361–367.
17. Quick HH, Vogt FM, Maderwald S, Herborn CU, Bosk S, Gohde S, Debatin JF, Ladd ME. High spatial resolution whole-body MR angiography featuring parallel imaging: initial experience. *Rofo Fortschr Geb Rontgenstr Neuen Bildgeb Verfahr* 2004;176:163–169.
18. Willinek WA, Gieseke J, von Falkenhausen M, Neuen B, Schild HH, Kuhl CK. Sensitivity encoding for fast MR imaging of the brain in patients with stroke. *Radiology* 2003;228:669–675.
19. Murphy BW, Carson PL, Ellis JH, Zhang YT, Hyde RJ, Chenvert TL. Signal-to-noise measures for magnetic resonance imagers. *Magn Reson Imaging* 1993;11:425–428.
20. Firbank MJ, Coulthard A, Harrison RM, Williams ED. A comparison of two methods for measuring the signal to noise ratio on MR images. *Phys Med Biol* 1999;44:N261–N264.

21. Determination of signal-to-noise ratio (SNR) in diagnostic magnetic resonance imaging. NEMA Standards Publication MS 1-2001.
22. Reeder SB, Wintersperger BJ, Dietrich O, Lanz T, Greiser A, Reiser MF, Glazer GM, Schoenberg SO. Practical approaches to the evaluation of signal-to-noise ratio performance with parallel imaging: application with cardiac imaging and a 32-channel cardiac coil. *Magn Reson Med* 2005;54:748–754.
23. Kellman P, McVeigh ER. Image reconstruction in SNR units: a general method for SNR measurement. *Magn Reson Med* 2005;54:1439–1447.
24. Griswold MA, Jakob PM, Chen Q, Goldfarb JW, Manning WJ, Edelman RR, Sodickson DK. Resolution enhancement in single-shot imaging using simultaneous acquisition of spatial harmonics (SMASH). *Magn Reson Med* 1999;41:1236–1245.
25. Bodurka J, Ledden PJ, van Gelderen P, Chu R, de Zwart JA, Morris D, Duyn JH. Scalable multichannel MRI data acquisition system. *Magn Reson Med* 2004;51:165–171.
26. Griswold MA, Jakob PM, Heidemann RM, Nittka M, Jellus V, Wang J, Kiefer B, Haase A. Generalized autocalibrating partially parallel acquisitions (GRAPPA). *Magn Reson Med* 2002;47:1202–1210.
27. Griswold MA, Kannengiesser S, Heidemann RM, Wang J, Jakob PM. Field-of-view limitations in parallel imaging. *Magn Reson Med* 2004;52:1118–1126.
28. Bland JM, Altman DG. Statistical methods for assessing agreement between two methods of clinical measurement. *Lancet* 1986;1:307–310.
29. Bland JM, Altman DG. Comparing methods of measurement: why plotting difference against standard method is misleading. *Lancet* 1995;346:1085–1087.
30. McVeigh ER, Henkelman RM, Bronskill MJ. Noise and filtration in magnetic resonance imaging. *Med Phys*. 1985;12:586–591.
31. Edelstein WA, Bottomley PA, Pfeifer LM. A signal-to-noise calibration procedure for NMR imaging systems. *Med Phys* 1984;11:180–185.
32. Margosian P, Schmitt F, Purdy D. Faster MR imaging: imaging with half the data. *Health Care Instrum* 1986;1:195–197.
33. Larsson EG, Erdogmus D, Yan R, Principe JC, Fitzsimmons JR. SNR-optimality of sum-of-squares reconstruction for phased-array magnetic resonance imaging. *J Magn Reson* 2003;163:121–123.
34. Rice SO. Mathematical analysis of random noise. In: Wax N, ed. *Selected papers on noise and stochastic processes*. New York, NY: Dover Publications, 1954:133–294.
35. Holden JE, Halama JR, Hasegawa BH. The propagation of stochastic pixel noise into magnitude and phase values in the Fourier analysis of digital images. *Phys Med Biol* 1986;31:383–396.
36. Gudbjartsson H, Patz S. The Rician distribution of noisy MRI data. *Magn Reson Med* 1995;34:910–914. (Erratum in: *Magn Reson Med* 1996;36:332.)